Effects of Bridging Ligands on the Current−Potential Behavior and Interfacial Kinetics of Ruthenium-Sensitized Nanocrystalline TiO_2 Photoelectrodes†

Kristine Kilså, Elizabeth I. Mayo, Darius Kuciauskas,‡ Randy Villahermosa, Nathan S. Lewis,* Jay R. Winkler,* and Harry B. Gray*

Beckman Institute, California Institute of Technology, Pasadena, California 91125

Received: August 21, 2002; In Final Form: November 15, 2002

We have shown that $Ru^{II}(bpy)_2$(bpy-4-$(xylyl)_x$-≡-phenyl-COOH)$(PF_6)_2$ (abbreviated Rux, where $x = 0$, 1 or 2 xylyl groups; bpy = 2,2′-bipyridine) dyes can act as sensitizers for nanocrystalline TiO_2 in functional photoelectrochemical cells under simulated solar illumination, albeit with low efficiencies. Both the short-circuit photocurrent density and the open-circuit voltage decreased as x was increased. Electron injection (10^6-10^8 s^{-1}) was slightly faster for the $x = 0$ dye, but both recombination ($10^{-15}-10^{-13}$ cm^3 s^{-1}) and regeneration (10^4-10^6 s^{-1} for 10 mM I^-) were slightly faster for the $x = 2$ dye. We suggest that the lack of distance dependence is due to the flexible one-carboxyl attachment to the surface resulting in the Ru−TiO_2 electron-tunneling distance being very similar for $x = 0$, 1, and 2. For all of the Rux sensitizers, a relatively small potential was needed for generation of current in the dark, indicating that the reaction between electrons in TiO_2 and the I_3^-/I^- electrolyte solution is as favorable for the Rux sensitizers as for unmodified TiO_2 electrodes.

Dye-sensitized TiO_2 solar cells have attracted much attention for possible applications in photochemical solar energy conversion devices.[1,2] Energy conversion efficiencies of up to 10% have been achieved in solar cells constructed with Ru(4,4′-dicarboxylic acid-2,2′-bypyridine)$_2$$(NCS)_2$ (the "N3 dye", abbreviated herein as $Ru(H_2L')_2(NCS)_2$).[3,4] The high efficiency of this cell is due to significant overlap with the solar spectrum, rapid charge separation, and efficient dye regeneration. Recent work on $Ru(H_2L')_2(NCS)_2$-sensitized photoelectrodes has shown that electron transfer to nanocrystalline TiO_2 quenches a significant fraction of the excited-state population in less than 100 fs.[5] Furthermore, regeneration of the oxidized dye by I^- in acetonitrile competes favorably with recombination between the electrons in TiO_2 and the oxidized dye.[6] A model for some of the dynamic processes in such cells is shown in Scheme 1. Upon excitation (k_1), the dye can either decay to the ground state (k_{-1}) or inject an electron into TiO_2 (k_2). The oxidized dye is subsequently regenerated by the I_3^-/I^- electrolyte (k_5). Possible back reactions for the injected electrons are recombination with oxidized dye (k_3) or back transfer to the I_3^-/I^- electrolyte (k_4).

For dyes that are derivatives of $Ru(bpy)_3^{2+}$ (bpy = 2,2′-bipyridine), the lowest excited state is formed by a metal-to-ligand charge-transfer (MLCT) transition.[7] The lifetime of this excited state usually exceeds 500 ns;[7] thus, CT reactions as slow as 1−10 ns can produce near unit quantum yields for the initial charge separation. In such dyes, electron injection occurs from the ligand attached to TiO_2, whereas recombination occurs between an electron in TiO_2 and the oxidized Ru center.[1] The latter reaction can lower the efficiencies of TiO_2 solar cells.

SCHEME 1: Kinetics Processes of Dye-Sensitized TiO_2 Photoelectrodes: k_1, Excitation; k_{-1}, Deactivation; k_2, Injection; k_3, Recombination; k_4, Back Transfer; k_5, Regeneration

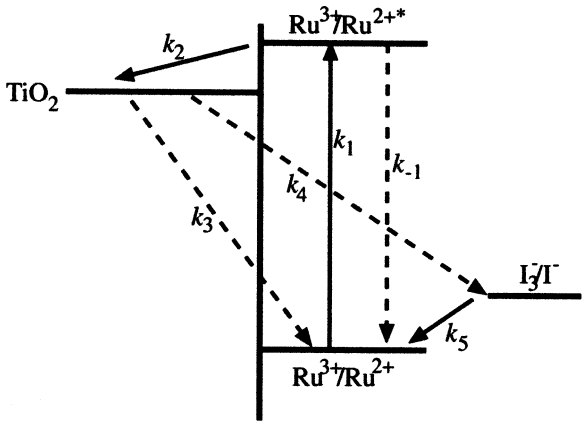

Hence, an attractive way to minimize this deleterious process would be to increase the distance between TiO_2 and the dye metal center, thereby decreasing the rate of recombination. Although the injection dynamics would also be slower, a high quantum yield for charge separation should be maintained.

Accordingly, we have prepared a series of dyes in which the distance between the ruthenium center and the anchoring group has been varied systematically. We describe herein the changes in steady-state and kinetics properties of dye-sensitized TiO_2 photoelectrodes that result from this increase in linker length between Ru and the TiO_2 surface. The dyes are derivatives of $Ru(bpy)_3^{2+}$ and have a single anchoring carboxyl group attached via a rigid linker to one of the bipyridine ligands. The dyes (shown below) are abbreviated Rux ($x = 0$, 1, 2), where x is the number of xylyl groups in the linker. Detailed descriptions of the syntheses of these dyes are provided elsewhere; NMR

† Part of the special issue "George S. Hammond & Michael Kasha Festschrift".

* To whom correspondence should be addressed. Phone: +1 626 395 6500. Fax: +1 626 449 4159. E-mail: hbgray@caltech.edu; winklerj@caltech.edu; nslewis@caltech.edu.

‡ Present address: Department of Chemistry, Virginia Commonwealth University, Richmond, VA 23284.

10.1021/jp021921u CCC: $25.00
Published on Web 04/11/2003

TABLE 1: Spectroscopic and Electrochemical Data

		MLCT						vs. SCE	
	R (Å)[a]	λ_{max}^{abs} (nm)[b]	λ_{max}^{ems} (nm)[b]	ϕ_{ems} (%)[b,c]	τ_{ems} (μs)[b,d]	k_0 (s^{-1})[b,e]	$\mathbf{E}_{00}$ (eV)[f]	$E^{\circ\prime}$ (V)[g]	$E^{\circ\prime}$* (V)[h]
Ru0	13.8	467	648	9.7	2.10	5×10^4	1.92	1.36	−0.56
Ru1	18.2	453	621	7.5	1.06	7×10^4	2.01	1.34	−0.67
Ru2	22.5	455	621	7.1	1.04	7×10^4	2.02	1.33	−0.69

[a] Distance (±0.2 Å) from MM2 calcualtions between the Ru metal center and carboxyl oxygens. [b] In degassed acetonitrile. [c] Emission quantum yields (±0.5%) measured relative to $Ru(bpy)_3Cl_2$ ($\phi_{ems} = 4.2\%$ in H_2O).[10] [d] Fitted to a single-exponential decay (±0.02 μs). [e] $k_0 = \phi_{ems}/\tau_{ems}$, where ϕ_{ems} is the emission quantum yield and τ_{ems} the lifetime of Rux. [f] 0−0 energy of the thermalized Ru(II) excited state obtained by fitting the emission spectra (±0.01 eV) to the theoretical expression reported by Caspar et al.[9] [g] Formal ground-state Ru^{III}/Ru^{II} reduction potential (±0.02 V) measured by cyclic voltammetry in acetonitrile with 0.1 M tetrabutylammonium hexafluorophosphate as supporting electrolyte vs ferrocene as internal standard. [h] Formal $Ru^{III}/*Ru^{II}$ reduction potential of the thermalized excited state, calculated as $E^{\circ\prime}* = E^{\circ\prime} - \mathbf{E}_{00}/q$, where q is the elementary charge.

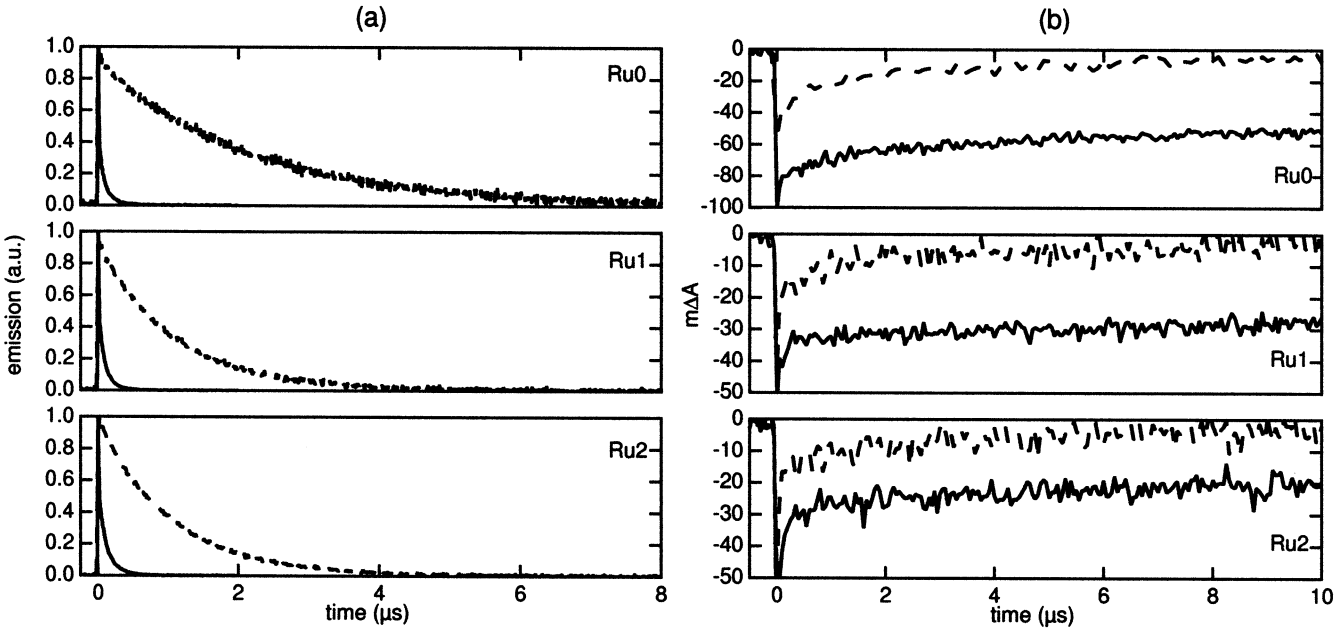

Figure 1. Emission and transient absorption kinetics for Rux dyes. $\lambda_{ex} = 480$ nm, $\lambda_{ems} = 630$ nm, and $\lambda_{ta} = 450$ nm. (a) Normalized emission decays of Rux in acetonitrile (- - -) and adsorbed on TiO_2 (—) in the presence of 0.50 M $LiClO_4$, 0.020 M pyridine, and 0.020 M pyridinium triflate in acetonitrile. (b) Transient absorption of Rux on TiO_2 in the presence of 0.50 M $LiClO_4$, 0.020 M pyridine, and 0.020 M pyridinium triflate in acetonitrile (—) and in the presence of 0.49 M $LiClO_4$, 0.010 M LiI, 0.020 M pyridine, and 0.020 M pyridinium triflate in acetonitrile (- - -). The differences in ΔA magnitude are mainly due to differences in ground-state absorption ($A_{450} = 0.7 \pm 0.2$).

and mass spectrometry were used to validate the compositions and structures of the complexes.[8]

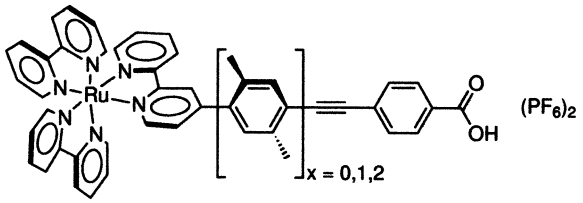

The solution photophysical behavior of Ru0 was found to differ slightly from that of the other sensitizers (Table 1). Both the absorption and emission spectra were red-shifted with the emission 0−0 transition energy[9] ($\mathbf{E}_{00}$) ~0.1 eV lower for Ru0. Although all of the radiative rate constants were similar, both the excited-state lifetime and the emission quantum yield[10] of Ru0 were greater than those of either Ru1 or Ru2. The excited-state lifetimes were all sufficiently long to ensure efficient charge separation, even for slow ($<10^7$ s^{-1}) electron-transfer processes. The Ru^{III}/Ru^{II} formal reduction potentials ($E^{\circ\prime}$) were nearly the same for all of the dyes, as the electronic cores around the metal centers are virtually identical. However, owing to differences in the 0−0 energy, the $Ru^{III}/*Ru^{II}$ potential ($E^{\circ\prime}*$) was found to be slightly more positive for Ru0. The excited-state energetics are comparable to those of other $Ru(bpy)_3^{2+}$-derivatives that exhibit efficient charge injection into the TiO_2 conduction band, with similar driving forces for this charge separation process.[11,12] The ground-state energetics imply that the oxidized dyes also have comparable driving forces for oxidation of I_3^-/I^- in a photoelectrochemical cell.

To investigate the interfacial kinetics of the dye-sensitized TiO_2 photoelectrodes, we measured rate constants for electron injection (k_2), recombination of injected electrons with the oxidized dye (k_3), and regeneration of the oxidized dye by iodide in the electrolyte (k_5) (Scheme 1) using nanosecond time-resolved spectroscopy. The energy of the TiO_2 conduction-band edge was fixed by controlling the H^+ and Li^+ activities.[6,12] The rate of reduction of I_3^-/I^- by electrons in the TiO_2 (k_4) was estimated from the potential required to produce a given amount of cathodic current density in the dark (vide infra).

To determine the rates of electron injection, we compared the Rux excited-state lifetimes in solution to those obtained when the dyes were bound to TiO_2. Clearly, adsorption to TiO_2 resulted in substantial quenching (Figure 1a). In degassed acetonitrile, Rux emission decays were single exponentials, but on TiO_2, the quenching dynamics exhibited multiexponential behavior (Table 2). This heterogeneity is probably due to different binding-site microenvironments. The data can be described satisfactorily by a sum of three exponentials. It is

TABLE 2: Rate Constants for Emission and Ground-State Recovery[a]

dye	k_{-1}^{MeCN} (s^{-1})[b]	$k_{-1}^{TiO_2}$ (s^{-1})[c,d]	k_2 (s^{-1})[e]	k'_3 (s^{-1})[c,f]	k_3 ($cm^3\ s^{-1}$)[g]	k'_5 (s^{-1})[d,h]
Ru0	4.8×10^5	1.1×10^8 (0.69)	1.1×10^8	4.8×10^6 (0.51)	1.1×10^{-13}	2.4×10^6 (0.58)
Ru0		1.4×10^7 (0.27)	1.4×10^7	3.3×10^4 (0.49)	7.6×10^{-16}	1.1×10^5 (0.42)
Ru0		4.5×10^6 (0.04)	4.0×10^6			
Ru1	9.4×10^5	1.1×10^8 (0.61)	1.0×10^8	5.0×10^6 (0.44)	1.2×10^{-13}	2.1×10^6 (0.78)
Ru1		1.3×10^7 (0.35)	1.2×10^7	5.3×10^4 (0.56)	1.2×10^{-15}	5.7×10^4 (0.22)
Ru1		4.7×10^6 (0.04)	3.8×10^6			
Ru2	9.6×10^5	9.9×10^7 (0.57)	9.8×10^7	8.8×10^6 (0.44)	2.0×10^{-13}	3.9×10^6 (0.44)
Ru2		1.1×10^7 (0.36)	9.5×10^6	7.7×10^4 (0.56)	1.8×10^{-15}	4.9×10^5 (0.39)
Ru2		4.2×10^6 (0.07)	3.2×10^6			1.9×10^4 (0.17)

[a] Estimated uncertainties are 25% in amplitudes and rate constants. [b] In degassed acetonitrile. [c] On TiO_2 with acetonitrile containing 0.50 M $LiClO_4$, and 0.020 M each of pyridine and pyridinium triflate. The amplitude of each term is given in parentheses. [d] Fitted to a sum of exponentials. [e] $k_2 = k_{-1}^{TiO_2} - k_{-1}^{CH_3CN}$. [f] According to eq 2. Amplitudes are in parentheses. [g] $k_3 = \Delta\epsilon d k'_3$ with $\Delta\epsilon d = 2.3 \times 10^{-18}\ cm^3\ mol^{-1}$ ($\Delta\epsilon$, difference in molar absorptivity; d, thickness of the TiO_2 film). [h] On TiO_2 with acetonitrile containing 0.49 M $LiClO_4$, 0.010 M LiI, 0.020 M pyridine, and 0.020 M pyridinium triflate. Amplitudes are given in parentheses.

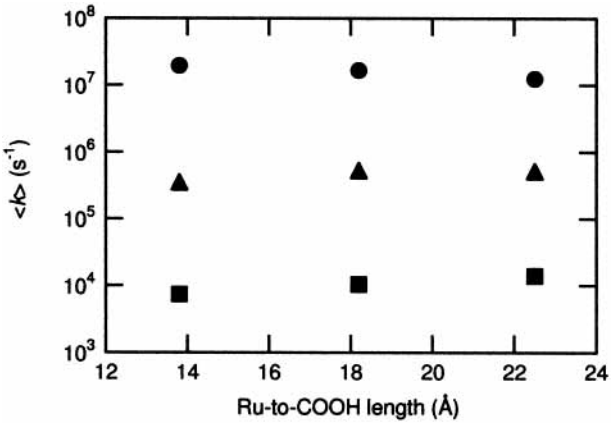

Figure 2. Integrated average rate constants (eq 1) for injection (●), recombination (■), and regeneration (▲) as a function of the Ru-to-COOH length. Injection rate constants ($\langle k_2 \rangle$, ●) obtained from the difference between the excited-state lifetimes of the dye in acetonitrile solution (single-exponential) and when bound to TiO_2 in the presence of 0.50 M $LiClO_4$, 0.020 M pyridine, and 0.020 M pyridinium triflate in acetonitrile ($\lambda_{ex} = 480$ nm and $\lambda_{ems} = 630$ nm). Recombination constants ($\langle k'_3 \rangle$, ■) of the oxidized dye with electrons in the TiO_2 from the time-resolved recovery of the ground state ($\lambda_{ex} = 480$ nm and $\lambda_{obs} = 450$ nm) for dyes bound to TiO_2 in the presence of 0.50 M $LiClO_4$, 0.020 M pyridine, and 0.020 M pyridinium triflate in acetonitrile. Regeneration rate constants ($\langle k'_5 \rangle$, ▲) of the oxidized dye with iodide from the time-resolved recovery of the ground state ($\lambda_{ex} = 480$ nm and $\lambda_{obs} = 450$ nm) for dyes bound to TiO_2 in the presence of 0.49 M $LiClO_4$, 0.010 M LiI, 0.020 M pyridine, and 0.020 M pyridinium triflate in acetonitrile. The uncertainties in the average rate constants are estimated to be 25%.

very likely that the fastest decay is itself a sum of decay processes, although this cannot be resolved as the shortest measurable lifetime was close to the width of the instrument response function (≈10 ns). Likewise, the amplitude of the fastest component is likely to be a lower limit. Numerical integration of normalized intensity profiles ($I(t)$) provided model-independent average rate constants for these nonexponential decays (eq 1)[13]

$$\langle k \rangle = \frac{1}{\int_0^\infty I(t)\, dt} \qquad (1)$$

The difference between the integrated emission decay on TiO_2 and in solution yields an average quenching rate constant ($\langle k_2 \rangle$). These quenching rates were only weakly dependent on linker length (Figure 2, Table 2); $\langle k_2 \rangle$ decreased by no more than a factor of 2 as the Ru-to-COOH distance increased from 13.8 to 22.5 Å.

The MLCT absorption bands of Rux dyes adsorbed onto TiO_2 were partially bleached following 450-nm laser excitation (Figure 1b). These signals, which persisted for more than 100 μs, can be attributed to the formation $Ru^{III}x$.[8] At low laser excitation powers, the relative magnitudes of the bleach signals ($\Delta A/A_{ground}$) for the three Rux dyes were all within a factor two and were comparable to that measured for a dye ($Ru(H_2L')_3^{2+}$) known to inject electrons into TiO_2 with high quantum efficiency.[12] At high laser excitation powers, the transient absorption signals saturated, presumably because of complete excitation of the Rux dyes. The magnitudes of these saturation signals can be used to estimate lower limits to the electron-injection quantum yields: $\Phi_{inj} \geq -\Delta A_{sat}/A_{ground}$. For the Rux ($x = 0$, 1, 2) series, the lower limits on the electron injection quantum yields are 0.09, 0.07, and 0.07, respectively. These values were calculated to be comparable to that obtained under similar conditions with $Ru(H_2L')_3^{2+}$ (0.07).[11] Estimated Φ_{inj} values correspond only to those species that persist on time scales longer than 10 ns; subnanosecond electron−hole recombination events could not be detected and would reduce the magnitude of the $Ru^{III}x$ signal. These transient absorption measurements suggest that Rux quenching on TiO_2 arises from high-quantum-yield electron injection into the semiconductor particles and that efficient photoelectrochemical cells for energy conversion applications might be fashioned from these dyes.

The kinetics of nongeminate charge recombination between electrons in TiO_2 and the oxidized dye were investigated by monitoring the recovery of the ground-state MLCT absorption. In accord with the behavior observed previously for $Ru(H_2L')_2(NCS)_2$-sensitized TiO_2 photoelectrodes, the recovery was fitted to a sum of two equal-concentration second-order kinetics functions:[6]

$$-\Delta A = \frac{a_i}{1 + a_i k'_{3i} t} + \frac{a_j}{1 + a_j k'_{3j} t} \qquad (2)$$

In eq 2, a relates absorbance and concentration, and the recombination constants (k'_3) have units of s^{-1}. For each sensitizer, the ratio of the fractions of the two populations ($a_i/(a_i + a_j)$ and $a_j/(a_i + a_j)$) was approximately 1:1. Because the samples were heterogeneous, there could be many more reaction rates, but their inclusion was not necessary to obtain satisfactory fits.

The k'_3 recombination constants were converted to true second-order rate constants using the thickness of the film and the ground-state molar absorptivity (Table 2).[6] However, because these factors were essentially equal for all three sensitizers ($x = 0$, 1, 2), the relative distance dependence of k_3 was the same

as that of k'_3. For both the slow and fast reaction processes, the corresponding rate constants increased slightly with increasing linker length. However, it should be noted that the differences may be within the experimental uncertainties. Average recombination constants ($\langle k'_3 \rangle$, eq 1) for each dye are plotted in Figure 2 as a function of Ru-to-COOH distance. Because back electron transfer occurs from TiO_2 to the Ru center, we would expect a significant decrease in rate as x increases, rather than the little to no increase observed.[14] The likely explanation for this finding is that the single anchoring group on Rux makes the connection to TiO_2 flexible, allowing the sensitizer to approach the surface and thereby decreasing the Ru−TiO_2 electron-tunneling distance. The flexibility in the linker could also contribute to the shallow distance dependence of the injection rates.

An analogous trend in rates was observed for the regeneration of the oxidized dye by iodide in the electrolyte. The recovery of the MLCT absorption following pulsed-laser excitation accelerated significantly when iodide was added to the electrolyte (Figure 1b). Fitting the data to a sum of two or three exponentials produced a minimum ensemble of [I^-]-dependent rate constants (k'_5) (Table 2). The dependence of average regeneration rate constants ($\langle k_5 \rangle$, eq 1) on the Ru-to-COOH distance is shown in Figure 2. For each complex, a 0.010 M I^- solution regenerated the reduced dye competitively with recombination from injected electrons (Figure 1b). Again, the fastest reaction was found for Ru2-sensitized TiO_2 photoelectrodes. This behavior could indicate that the assumed flexibility and resultant sensitizer interaction with the surface is affecting the iodide oxidation. Flash/quench experiments were also performed on the unbound dyes in acetonitrile, using methyl viologen as the electron acceptor to generate the Ru^{III} form of the dyes. The pseudo-first-order rate constants for reduction of the oxidized dyes by iodide under these conditions were essentially identical for all three dyes, with $k'_5 = 2 \times 10^5\ s^{-1}$ for $[I^-] = 1.0 \times 10^{-5}$ M. Importantly, regeneration was observed to be significantly faster when the dyes were free in solution than when they were bound to TiO_2.

The emission decay of Rux on TiO_2 is much faster than in solution, implying that electron injection is still efficient, although a minor fraction of the excited-state population injected slowly. Given that injection of electrons into TiO_2 was much faster than excited-state decay, and that regeneration competed effectively with recombination, it is surprising that Rux-sensitized TiO_2 photoelectrodes are not more efficient (Figure 3, Table 3). The overlap of the Rux MLCT absorption with the solar spectrum is not very favorable; thus, solar cells containing these dyes are expected to be less efficient than $Ru(H_2L')_2(NCS)_2$-sensitized solar cells. On the basis of the similarities with the absorption spectrum of $Ru(H_2L')_3^{2+}$, we would expect Rux solar cell efficiencies to be comparable to that of $Ru(H_2L')_3^{2+}$-sensitized TiO_2.[15] However, the remarkably similar interfacial kinetics observed for the Rux dyes fail to explain the large differences in their photoelectrochemical behavior. The limiting photocurrent densities under simulated solar illumination depended strongly on the linker length in the Rux series (Figure 3, Table 3). The short-circuit current density (J_{sc}) decreased by approximately a factor of 2 for $\Delta x = 1$. At such low current densities, it is not unusual to observe some hystersis at these scan rates (20 mV s^{-1}). The decrease in J_{sc} cannot be explained by a change in light absorption of the various complexes, as the spectra of the adsorbed dyes are very similar. The quantum yield for conversion of absorbed photons to current was less than 0.1 for all three dyes, and the quantum yield decreased with increasing linker length (Table 3). Also, the magnitude of the open-circuit voltage (V_{oc}) decreased with linker length (Table 3). Part of the decrease in V_{oc} with increasing x is attributable to the lower photocurrent density produced by Ru1 and Ru2. Overall, the J_{sc}, V_{oc}, and shape of the current density-potential curve (Figure 3) for the Rux dyes gave low photoelectrode energy conversion efficiencies (Table 3) under 100 mW cm^{-2} of simulated Air Mass 1.0 solar illumination conditions. The performance of these photoelectrodes can be compared to that of a $Ru(bpy)_3^{2+}$ derivative in which a single carboxyl groups is directly attached to one of the bipyridine ligands. The value of J_{sc} for this compound was 4 times higher than for Ru0, and the magnitude of V_{oc} was slightly higher as well.[11] Clearly, placing any one of the linkers ($x = 0, 1, 2$) between TiO_2 and the Ru center has a negative effect on photoelectrode performance.

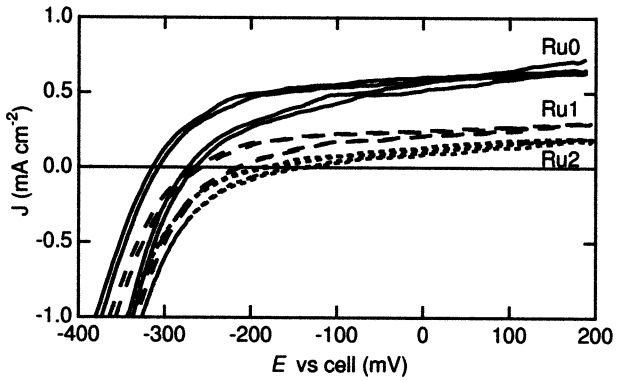

Figure 3. Current density−potential characteristics for TiO_2 sensitized with Ru0 (—), Ru1 (- - -), and Ru2 (···), respectively ($A_{MLCT} = 1.5 \pm 0.3$). The data (corrected for uncompensated cell resistance, 64 ohms) were measured under simulated Air Mass 1.0 100 mW cm^{-2} conditions in a potentiostatic three-electrode apparatus at 20 mV s^{-1} scan rate between +0.20 and −0.60 V vs the Nernstian potential of the cell. Two consecutive scans in each direction are shown for each dye. The electrolyte was acetonitrile containing 0.50 M LiI, 0.040 M I_2, 0.020 M pyridine, and 0.020 M pyridinium triflate.

TABLE 3: Photoelectrochemical Data[a]

	Air Mass 1.0				dark
	J_{sc} (mA cm^{-2})[b]	V_{oc} (V)[c]	efficiency (%)[d]	Ext. QY[e]	V_{dark} (V)[f]
Ru0	0.59	−0.29	0.1	0.09	−0.23
Ru1	0.23	−0.24	0.03	0.03	−0.23
Ru2	0.11	−0.16	0.004	0.02	−0.16

[a] The electrolyte was acetonitrile containing 0.50 M LiI, 0.040 M I_2, and 0.020 M each of pyridine and pyridinium triflate. [b] Estimated uncertainties are ± 0.05 mA cm^{-2}. [c] Estimated uncertainties are ± 0.03 V. [d] Calculated as P_{max}/P_{light}, where $P_{light} = 100$ mW cm^{-2} and P_{max} is the largest value of $-(J \times V)$. [e] Calculated as the ratio of the observed J_{sc} to the value expected for a unity quantum yield when the measured absorbance of the dyes on TiO_2 electrodes are convoluted with the spectral irradiance of the solar simulator between 1100 and 360 nm. [f] Estimated uncertainties are ± 0.05 V.

The back reaction that determines the photovoltage in sensitized TiO_2 systems is electron transfer from nanocrystalline TiO_2 to oxidized species in the I_3^-/I^- electrolyte solution (represented by the rate process k_4 in Scheme 1).[16] Trends in the rate of this back reaction were evaluated from the forward-bias potential necessary to produce a fixed amount of cathodic dark current density (0.1 mA cm^{-2}) at the TiO_2−solution interface, where a less negative potential is indicative of more facile electron transfer between TiO_2 and the I_3^-/I^- electrolyte. Interestingly, the magnitudes of these potentials were similar for the three sensitizers (Table 3); thus, we would expect the rate of back transfer to be similar in each case. The potential required to drive 0.1 mA cm^{-2} of cathodic dark current density

for each Rux dye was less negative than for $Ru(H_2L')_3^{2+}$-sensitized TiO_2 (under low photocurrent density conditions),[12] which implies that the lower Rux efficiencies are in part due to enhanced electron transfer from TiO_2 to the solution redox couple. This conclusion is also supported by comparison with nonsensitized TiO_2 electrodes, which were observed to require -0.23 V to produce a cathodic current density of 0.1 mA cm^{-2} to the I_3^-/I^- electrolyte. These data indicate that the deleterious dark cathodic reduction of I_3^-/I^- by electrons in the TiO_2 as a result of adsorption of the monocarboxyl-xylyl linkers is similar, or even slightly accelerated, relative to that of unmodified TiO_2.

The present data indicate that even when injection and regeneration compete favorably with recombination in a dynamics experiment in the presence of I^- high quantum yields for photocurrent flow are not necessarily obtained at steady state in a photoelectrochemical cell containing I_3^-/I^-. This behavior suggests that, for the long linkers species resulting from the addition of I_3^- are present under steady-state conditions that deleteriously increase the ratio of recombination and/or excited-state quenching relative to regeneration. It is possible that the presence of triiodide in the current density-potential experiments plays a crucial role in the interfacial kinetics of these systems.

In summary, we have shown that ruthenium-based dyes with one carboxyl anchoring group and various xylyl-linker lengths sensitize nanocrystalline TiO_2. Despite the small overlap with the solar spectrum, the dyes function in photoelectrochemical cells under simulated solar illumination, albeit with low efficiencies and with photocurrent densities that decrease with linker length. Injection is slightly faster for Ru0, but both recombination and regeneration are faster for Ru2, although the variation in the dynamics among the dyes is less than a factor of 2. The measured kinetics do not satisfactorily explain the low efficiencies, nor the trends among the steady-state photoelectrochemical behavior of the dyes, and suggest that there are other possible quenching mechanisms or electron-transfer processes which are not included in the current kinetics model. We suggest that the $Ru-TiO_2$ electron tunneling distance is roughly the same for $x = 0$, 1, and 2, as the one-carboxyl attachment to the surface is flexible enough for the Ru center to approach the TiO_2 surface in all three cases. Furthermore, electron transfer from Rux sensitized TiO_2 to I_3^-/I^- is more pronounced than for $Ru(H_2L')_3^{2+}$-sensitized as well as unsensitized photoelectrodes, in accord with the lower efficiencies of the Rux-based cells.

Acknowledgment. K.K. thanks the Carlsberg Foundation, Denmark, for a postdoctoral fellowship, and R.V. acknowledges the Link Foundation for funding. This work is supported through NREL subcontract (ACQ-1-30619-09) under DOE contract (DE-AC36-99-G010337). Work on the synthesis and characterization of the Rux complexes was supported by the NSF (H.B.G. and J.R.W.) and by the Arnold and Mabel Beckman Foundation.

References and Notes

(1) Hagfeldt, A.; Grätzel, M. *Chem. Rev.* **1995**, *95*, 49−68.
(2) Cahen, D.; Hodes, G.; Grätzel, M.; Guillemoles, J. F.; Riess, I. *J. Phys. Chem. B* **2000**, *104*, 2053−2059.
(3) O'Regan, B.; Grätzel, M. *Nature* **1991**, *353*, 737−740.
(4) Nazeeruddin, M. K.; Kay, A.; Rodicio, I.; Humphry-Baker, R.; Müller, E.; Liska, P.; Vlachopoulos, N.; Grätzel, M. *J. Am. Chem. Soc.* **1993**, *115*, 6382−6390.
(5) Benkö, G.; Kallioinen, J.; Korppi-Tommola, J. E. I.; Yartsev, A. P.; Sundström, V. *J. Am. Chem. Soc.* **2002**, *124*, 489−493.
(6) Kuciauskas, D.; Freund, M. S.; Gray, H. B.; Winkler, J. R.; Lewis, N. S. *J. Phys. Chem. B* **2001**, *105*, 392−403.
(7) Roundhill, D. M. Photochemistry, Photophysics, and Photoredox Reactions of $Ru(bpy)_3^{2+}$ and Related Compounds. *Photochemistry and Photophysics of Metal Complexes*; Plenum Press: New York, 1994; Chapter 5.
(8) Villahermosa, R. Ph.D. Thesis, California Institute of Technology, Pasadena, CA, 2002.
(9) Caspar, J. V.; Westmoreland, T. D.; Allen, G. H.; Bradley, P. G.; Meyer, T. J.; Woodruff, W. H. *J. Am. Chem. Soc.* **1984**, *106*, 3492−3500.
(10) van Houten, J.; Watts, R. J. *J. Am. Chem. Soc.* **1976**, *98*, 4853−4858.
(11) Kilså, K.; Mayo, E. I.; Lewis, N. S.; Winkler, J. R.; Gray, H. B. In preparation.
(12) Sauvé, G.; Cass, M. E.; Coia, G.; Doig, S. J.; Lauermann, I.; Pomykal, K. E.; Lewis, N. S. *J. Phys. Chem. B* **2000**, *104*, 6821−6836.
(13) Maroncelli, M.; Fleming, G. R. *J. Chem. Phys.* **1987**, *86*, 6221−6239.
(14) Ponce, A.; Gray, H. B.; Winkler, J. R. *J. Am. Chem. Soc.* **2000**, *122*, 8187−8191.
(15) Electron injection and recombination kinetics also have been studied in nanocrystalline TiO_2 sensitized with tripodal Ru^{II}-spacer complexes (Galoppini, E.; Guo, W.; Zhang, W.; Hoertz, P. G.; Qu, P.; Meyer, G. J. *J. Am. Chem. Soc.* **2002**, *124*, 7801−7811) and Ru^{II}(4,4′-di-(*p*-carboxyphenyl)-2,2′-bipyridine)$_n$ (4,4′-dimethoxy-2,2′-bipyridine)$_{3-n}$ (n = 1,2,3) (Kalyanasundaram, K.; Nazeeruddin, M. K.; Grätzel, M.; Viscardi, G.; Savarino, P.; Barni, E. *Inorg. Chim. Acta* **1992**, *200*, 831−839).
(16) Huang, S. Y.; Schlichthörl, G.; Nozik, A. J.; Grätzel, M.; Frank, A. J. *J. Phys. Chem. B* **1997**, *101*, 2576−2582.